J. Cent. South Univ. (2020) 27: 2515−2529
DOI: https://doi.org/10.1007/s11771-020-4477-9

Springer

Electrochemically exfoliated graphene as high-performance catalyst support to promote electrocatalytic oxidation of methanol on Pt catalysts

YUAN Xu(袁旭), YUE Wen-bo(岳文博), ZHANG Jin(张锦)

Beijing Key Laboratory of Energy Conversion and Storage Materials, College of Chemistry, Beijing Normal University, Beijing 100875, China

Abstract: Electrochemically exfoliated graphene (EEG) is a kind of high-quality graphene with few oxygen-containing functional groups and defects on the surface, and thereby is more suitable as catalyst support than other carbon materials such as extensively used reduced graphene oxide (rGO). However, it is difficult to grow functional materials on EEG due to its inert surface. In this work, ultra-small Pt nanocrystals (~2.6 nm) are successfully formed on EEG and show better electrocatalytic activity towards methanol oxidation than Pt catalysts on rGO. The outstanding catalytic properties of Pt catalysts on EEG can be attributed to the fast electron transfer through EEG and high quality of Pt catalysts such as small grain size, high dispersibility and low oxidation ratio. In addition, SnO_2 nanocrystals are controllably generated around Pt catalysts on EEG to raise the poison tolerance of Pt catalysts through using glycine as a linker. Owing to its outstanding properties such as high electrical conductivity and mechanical strength, EEG is expected to be widely used as a novel support for catalysts.

Key words: electrochemically exfoliated graphene; platinum; tin dioxide; glycine; methanol oxidation

Cite this article as: YUAN Xu, YUE Wen-bo, ZHANG Jin. Electrochemically exfoliated graphene as high-performance catalyst support to promote electrocatalytic oxidation of methanol on Pt catalysts [J]. Journal of Central South University, 2020, 27(9): 2515−2529. DOI: https://doi.org/10.1007/s11771-020-4477-9.

1 Introduction

Energy shortage and environmental pollution have become two urgent problems in the world nowadays. The development of pollution-free new energy is essential to solve the serious environmental pollution and energy crisis. As a newly emerging energy conversion device, direct methanol fuel cells (DMFCs) possess many advantages such as high energy density, operational safety and pollution-free, and thus are widely applied in automobile and aerospace industries [1, 2]. The performance of DMFCs is highly relied on the electrochemical properties of electrode materials. Up to now, platinum is still the most efficient catalyst material for methanol oxidation [3, 4]. However, the traditional commercial Pt/C catalyst is not able to satisfy the demand for high energy-density batteries [5, 6]. A novel catalyst support is urgently needed to further increase the electrocatalytic activity, durability and utilization of Pt catalysts. Graphene is a novel two-dimensional carbon nanomaterial that has advantages of large surface area, high electrical and thermal conductivity, and remarkable mechanical property [7]. Therefore, graphene is regarded as a high-performance catalyst support, which can dramatically enhance the catalytic activities of catalysts [8−10]. So far, rGO derived from graphene

Foundation item: Projects(21573023, 21975030) supported by the National Natural Science Foundation of China
Received date: 2019-10-26; **Accepted date:** 2020-08-10
Corresponding author: YUE Wen-bo, PhD, Professor; Tel: +86-10-58804229; E-mail: wbyue@bnu.edu.cn; ORCID: https://orcid.org/0000-0003-3809-6733

oxide (GO) is usually used as the catalyst support rather than pristine graphene because GO can be mass-produced from graphite [11], and the oxygen-containing groups of GO such as hydroxyl and carboxyl could act as nucleation sites for the growth of Pt crystals [12, 13]. However, lots of residual defects on the rGO surface cause the performance degradation of rGO, even though the functional groups of GO are eliminated [14, 15]. Thus rGO is not an ideal graphene substrate for catalysts, and high-quality graphene which can be mass-produced is earnestly desired to replace rGO as the catalyst support.

Recently, a modified electrochemical exfoliation method is employed in the mass production of high-quality graphene [16, 17]. Compared to rGO, EEG displays better electrical conductivity and mechanical strength. Thus it is believed that using EEG as a catalyst carrier instead of rGO can enhance the catalytic activity of Pt. However, fabrication of functional materials on EEG is more difficult than on GO because EEG nanosheets with hydrophobic surface tend to aggregate in water through π-π interaction. Thus polar aprotic solvents such as *N*,*N*-dimethylformamide (DMF) are usually adopted to disperse EEG, which limits the synthetic routes. In addition, lack of nucleation sites is not beneficial to the nucleation and growth of crystals on the surface of EEG. In our previous work, some metal oxide nanocrystals directly grew on EEG through a solvothermal method and exhibit superior electrochemical performance in comparison with rGO supported metal oxides [18,19]. A new growth mechanism differing from the traditional crystal growth mechanism is also proposed. The results show that the formation of polymerized precursors is greatly important for the formation of nanoparticles on EEG.

In this work, Pt nanocrystals with an average particle size of ~2.6 nm are successfully synthesized on EEG by reduction of Pt-containing precursors in hot ethylene glycol. Compared to the traditional synthesis in DMF, ethylene glycol acts as both the solvent and the reducing agent, which supplies a mild reduction environment for the formation of Pt nanoparticles. In contrast, Pt nanoparticles show a larger particle size (~5.4 nm) and tend to aggregate on rGO under the same synthesis conditions. Compared to Pt nanoparticles on rGO (rGO-Pt-eg), Pt nanoparticles on EEG (EEG-Pt-eg) show superior catalytic properties for methanol oxidation, demonstrating that EEG is a superior carbon carrier for Pt catalysts. In addition, SnO_2 nanocrystals are formed around Pt nanoparticles on EEG to further improve the poison tolerance of Pt catalysts. As a catalyst promoter, SnO_2 can adsorb hydroxyl radicals on its surface, which further oxidizes carbonaceous intermediates to carbon dioxide [20, 21]. Therefore, the catalytic properties of EEG-Pt-eg are further enhanced by cooperation with SnO_2. EEG as a novel graphene substrate is promising to be widely applied in the field of energy conversion and catalysis.

2 Experimental

2.1 Sample preparation

1) EEG-Pt-eg and rGO-Pt-eg. EEG was synthesized on the basis of the literature reports [16, 17]. EEG-Pt-eg was synthesized by reduction of chloroplatinic acid in ethylene glycol solution. In brief, 0.03 g of EEG was dispersed in 50 mL of ethylene glycol with ultrasonication for 5 h, and 0.02 g of $H_2PtCl_6·6H_2O$ was then dissolved in this solution under agitation. The suspension was reflux-heated in an oil bath at 160 °C for 3 h. The powder was collected by centrifugation, washed with ethanol, and vacuum-dried at 60 °C overnight. rGO-Pt-eg was synthesized by the same method except that equal-mass GO was used instead of EEG.

2) EEG-SnO_2@Pt and EEG-SnO_2/Pt. EEG-based SnO_2 was first synthesized according to our previous work [18]. In brief, 0.03 g of EEG was dispersed in 60 mL of DMF. 0.08 g of $SnCl_4·5H_2O$ and 0.02 mL of distilled water were then added into this solution under stirring for 0.5 h. The solution was poured into a 100 mL Teflon-lined stainless steel autoclave and heated at 160 °C for 12 h. The powder was collected by centrifugation, washed with ethanol, and dried at 60 °C. Subsequently, the as-synthesized EEG-SnO_2 was dispersed in 50 mL of ethylene glycol with ultrasonication for 5 h, followed by addition of 0.05 g of glycine under agitation. The glycine-coated EEG-SnO_2 was collected by centrifugation and then added to 50 mL of ethylene glycol. 0.02 g of $H_2PtCl_6·6H_2O$ was also added into this solution with stirring for 0.5 h. The suspension was reflux-heated in an oil bath at

160 °C for 3 h. The powder was collected by centrifugation, washed with ethanol, and vacuum-dried at 60 °C overnight. For comparison, EEG-SnO_2@Pt was also prepared without using glycine and denoted as EEG-SnO_2/Pt.

2.2 Sample characterization and measurement

Characterization and measurement methods were reported previously and thereby supplied in the supporting information [7, 12].

3 Results and discussions

3.1 Structure and morphological characterization of EEG-Pt-eg and rGO-Pt-eg

The overall synthetic processes of EEG-Pt-eg, rGO-Pt-eg and EEG-SnO_2@Pt are shown in Figure 1. The Pt-containing precursor (H_2PtCl_6) is firstly attached to EEG or GO and then reduced to Pt nanoparticles by ethylene glycol. Meanwhile, GO is also reduced to rGO by ethylene glycol. Considering that oxygen-containing groups of GO could serve as nucleation sites for the crystal growth, Pt nanocrystals are preferentially formed around the defects of GO and gradually grow into larger particles. On the contrary, lack of preferential nucleation sites results in the uniform distribution of Pt nanoparticles on the surface of EEG. EEG-SnO_2 was prepared prior to the synthesis of EEG-SnO_2@Pt. According to our previous work [18], Sn^{4+} ions are first hydrolyzed with a little water to form large polymerized clusters. These polymerized clusters are then adsorbed on the EEG surface via inter-molecular interactions and decomposed into SnO_2 nanoparticles under solvothermal treatment. Subsequently, glycine is absorbed on the hydrophilic surface of SnO_2 nanoparticles and the excess glycine is washed away. The NH_2 groups of glycine induce the nucleation of Pt crystals on the surface of SnO_2. Finally, Pt nanocrystals are formed around SnO_2 nanoparticles on EEG.

To investigate the superior properties of EEG in comparison with rGO, EEG-Pt-eg and rGO-Pt-eg were firstly observed by SEM and TEM. SEM images (Figures 2(a) and (b)) reveal that small Pt nanocrystals are uniformly distributed on the surface of EEG, whereas large Pt nanoparticles and agglomerates are loaded on rGO under the same synthesis conditions. TEM images (Figures 2(c) and (d)) also show that Pt catalysts have smaller particle size and better dispersion on EEG. The different growth behaviors of Pt nanocrystals on EEG and rGO may result from the different surface structure between EEG and GO. Compared to EEG, GO possesses plenty of functional groups and defects on the surface, which can provide ample active sites for the nucleation and growth of Pt nanocrystals. On the contrary, Pt-containing precursors are homogeneously adsorbed on EEG and grow to Pt clusters because of lacking preferential nucleation sites on EEG. To gain more insight into the formation of Pt nanocrystals on EEG, EEG is mixed with $H_2PtCl_6·6H_2O$ in ethylene glycol, and the solid sample (EEG-H_2PtCl_6) was collected by centrifugation. The Pt and Cl peaks appear in the EDX spectrum of EEG-H_2PtCl_6 (Figure S1(a)), indicating that H_2PtCl_6 molecules prefer to adsorb on the EEG surface. Furthermore, SEM-EDX mapping images (Figures S1(b)−(f)) show that the distribution of Pt and Cl elements overlaps with that of C element, confirming the uniform adsorption of

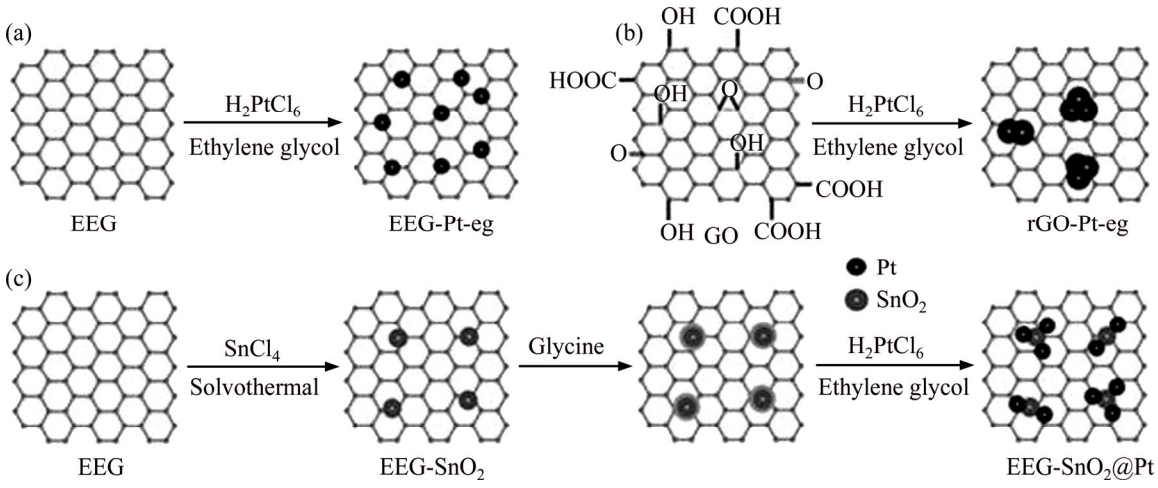

Figure 1 Schematic illustration of synthesis routes for: (a) EEG-Pt-eg; (b) rGO-Pt-eg; (c) EEG-SnO_2@Pt

H_2PtCl_6 molecules on EEG. The particle size distribution of Pt catalysts (Figure S2) shows that the average diameter of Pt nanocrystals on EEG is ~2.6 nm, much smaller than that on rGO (~5.4 nm). It means that the crystal growth of Pt nanocrystals is suppressed on EEG, which could dramatically affect their electrocatalytic activity towards methanol oxidation. The spacing of the lattice fringes observed in HRTEM images (Figures 2(e) and (f)) is ~0.226 nm, close to the *d*-spacing of (111) plane of Pt. More importantly, the *d*-spacing of ~0.215 nm that corresponds to the (100) plane of graphite is visible in the HRTEM image of EEG-Pt-eg (Figure 2(e)), indicative of the pristine regions of EEG with few defects [19, 22]. The hexagonal lattice of graphene was not observed in HRTEM images of rGO-Pt-eg (Figure 2(f)), which is attributed to the defects throughout the surface of rGO. The surface defects of graphene are not conducive to the homogeneous nucleation and growth of Pt nanoparticles.

The crystal phases of EEG-Pt-eg and rGO-Pt-eg were identified by XRD. All broad peaks in the XRD patterns (Figure 3(a)) are indexed into the cubic structure of Pt (JCPDS No. 87-0646), suggesting the successful synthesis of Pt nano-

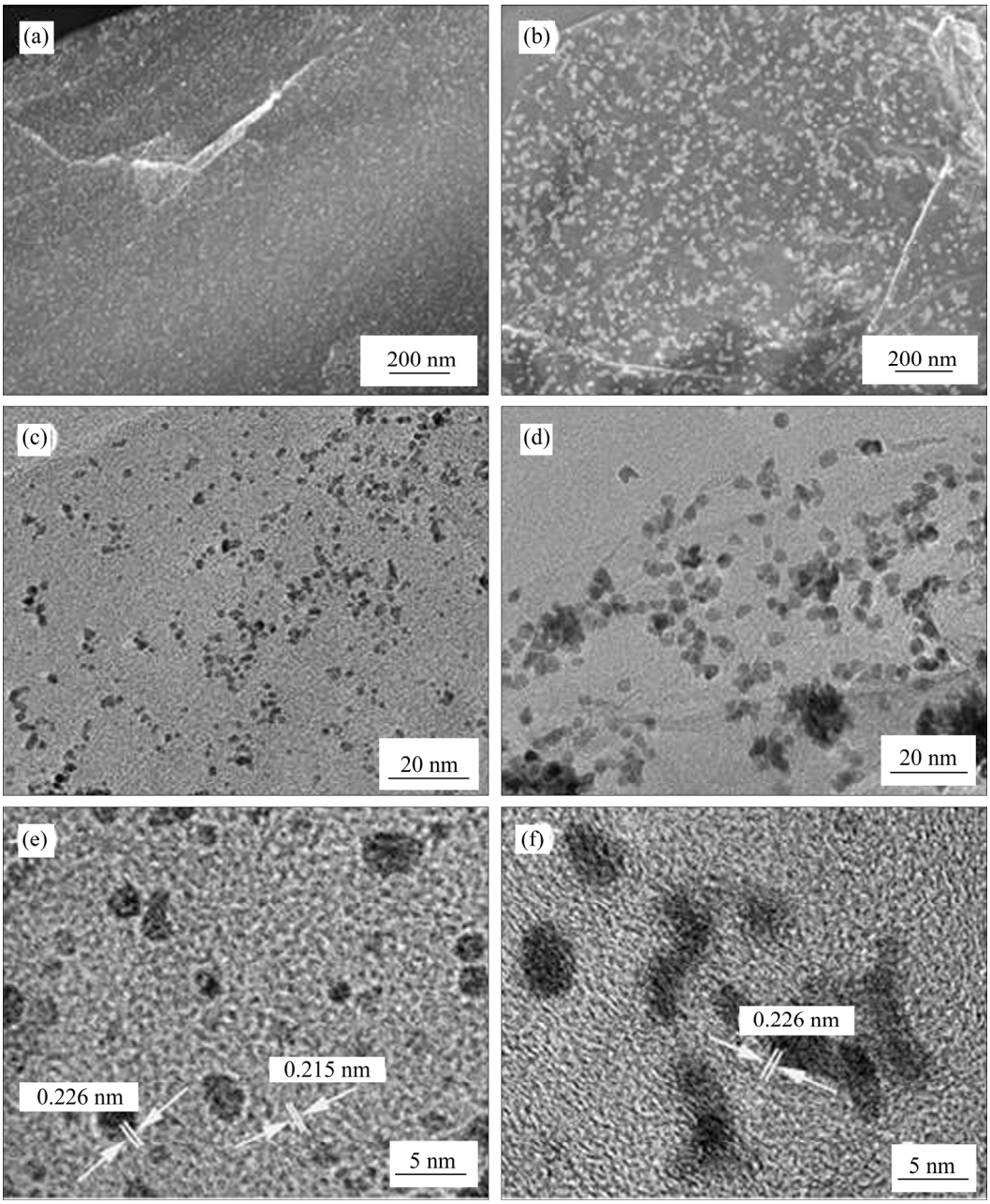

Figure 2 SEM, TEM and HRTEM images of EEG-Pt-eg (a, c, e) and rGO-Pt-eg (b, d, f) (The *d*-spacings of the marked fringes in (e, f) are ca. 0.226 nm, corresponding to the (111) plane of cubic Pt)

particles on EEG or rGO. Furthermore, the XRD pattern of EEG-Pt-eg shows wider peaks in comparison with that of rGO-Pt-eg, indicating smaller Pt nanocrystals formed on EEG. Besides these characteristic peaks, the peak corresponding to the basal spacing of stacked EEG (26.5°) or rGO (23.8°) is also detected in XRD patterns. The interlayer spacing of stacked EEG nanosheets is ~0.336 nm, which is very close to that of pristine graphite (0.335 nm), but smaller than that of stacked rGO nanosheets (~0.373 nm). It is indicated that some functional groups still remain on the surface of rGO after reduction of GO in hot ethylene glycol.

The residual surface groups and defects of EEG-Pt-eg and rGO-Pt-eg were further determined by FT-IR and Raman. The characteristic absorption bands which are assigned to the stretching vibrations of C—O, C—OH, O—H, C═O and the skeletal vibration of C═C are detected in the FT-IR spectrum of GO (Figure S3(a)), illustrating that GO possesses several oxygen-containing functional groups such as hydroxyl, carbonyl or epoxide groups [23, 24]. On the contrary, the spectrum of EEG shows vanished C—O and C═O bands and weaker C—OH band, demonstrating that only a small number of functional groups are generated on the surface of EEG during electrochemical exfoliation of graphite. Raman spectra of GO and EEG (Figure S3(b)) show two prominent peaks related to the vibration of sp^3 carbon atoms of disordered graphite (the D band) and the in-plane vibration of sp^2 carbon atoms in a 2D hexagonal lattice (the G band) [25]. The number of defects on GO and EEG can be simply evaluated using the intensity ratio of D and G bands (I_D/I_G). The I_D/I_G value of EEG is ~0.32, much smaller than that of GO (1.04). Overall, as a promising catalyst carrier, EEG is lack of surface groups and defects, and the reduction process of GO to rGO is not necessary for EEG. The FT-IR spectra of EEG-Pt-eg and rGO-Pt-eg (Figure 3(b)) are similar to that of EEG, indicating that most of oxygen-containing groups of GO are eliminated in hot ethylene glycol. However, rGO still has plentiful surface defects (Figure 3(c)) based on the I_D/I_G value of rGO-Pt-eg (~0.92). The I_D/I_G value of EEG-Pt-eg increases to ~0.50 after loading of Pt catalysts, implying the formation of C-Pt bonds on EEG, but still smaller than that of rGO-Pt-eg. The residual defects on graphene have a tremendous impact on its electrical conductivity. The electrical conductivities of EEG-Pt-eg and rGO-Pt-eg were tested by a four-point probe technique [24]. Apparently, EEG-Pt-eg shows better electrical conductivity (33.8 S/cm) than rGO-Pt-eg (13.7 S/cm).

The surface characteristics of EEG-Pt-eg and rGO-Pt-eg were also investigated by XPS. Survey spectra of EEG-Pt-eg and rGO-Pt-eg (Figure 3(d)) display three element peaks involving Pt 4f, C 1s, Pt 4d and O 1s peaks. The intensity ratio of C 1s peak to O 1s peak is ~4.9 for EEG-Pt-eg, higher than that for rGO-Pt-eg (~3.9), also confirming that EEG has less oxygen-containing groups than rGO. The high-resolution Pt 4f XPS spectra of EEG-Pt-eg and rGO-Pt-eg (Figure 3(e)) display two main peaks at 71.6 and 74.9 eV that are assigned to the Pt $4f_{7/2}$ and Pt $4f_{5/2}$ of Pt^0. Two resolved peaks corresponding to the Pt $4f_{7/2}$ and Pt $4f_{5/2}$ of Pt^{2+} are also detected, reflecting the formation of tiny amount of PtO or $Pt(OH)_2$. It is worth noting that the ratio of Pt^0/Pt^{2+} for rGO-Pt-eg (7.9) is lower than that for EEG-Pt-eg (13.1). This may be due to the fact that GO possesses plenty of oxygen-containing groups, and thereby can oxidize Pt^0 to Pt^{2+} during the synthesis process, resulting in a decline in the methanol oxidation reaction (MOR) performance of rGO-Pt-eg. The C 1s peak can be further resolved into four peaks, which are associated with C═C, C—O, C═O and O—C═O groups, respectively [26,27]. The peaks related to C—O, C═O and O—C═O groups are too weak in the spectra of EEG-Pt-eg and rGO-Pt-eg (Figure 3(f)), which is in good accordance with the FT-IR results.

3.2 Electrochemical performance of EEG-Pt-eg and rGO-Pt-eg

The electrocatalytic properties of EEG-Pt-eg and rGO-Pt-eg were tested and compared in order to study the advantages of EEG as the catalyst support. The loadings of Pt in EEG-Pt-eg and rGO-Pt-eg are accurately measured by ICP analysis. The content of Pt in EEG-Pt-eg is ~17.6 wt%, which is similar to that in rGO-Pt-eg (18.3 wt%). Therefore, the effect of Pt loadings on the electrocatalytic activity can be ignored. The a electrochemically active surface areas (ECSAs) of EEG-Pt-eg and rGO-Pt-eg were firstly measured in

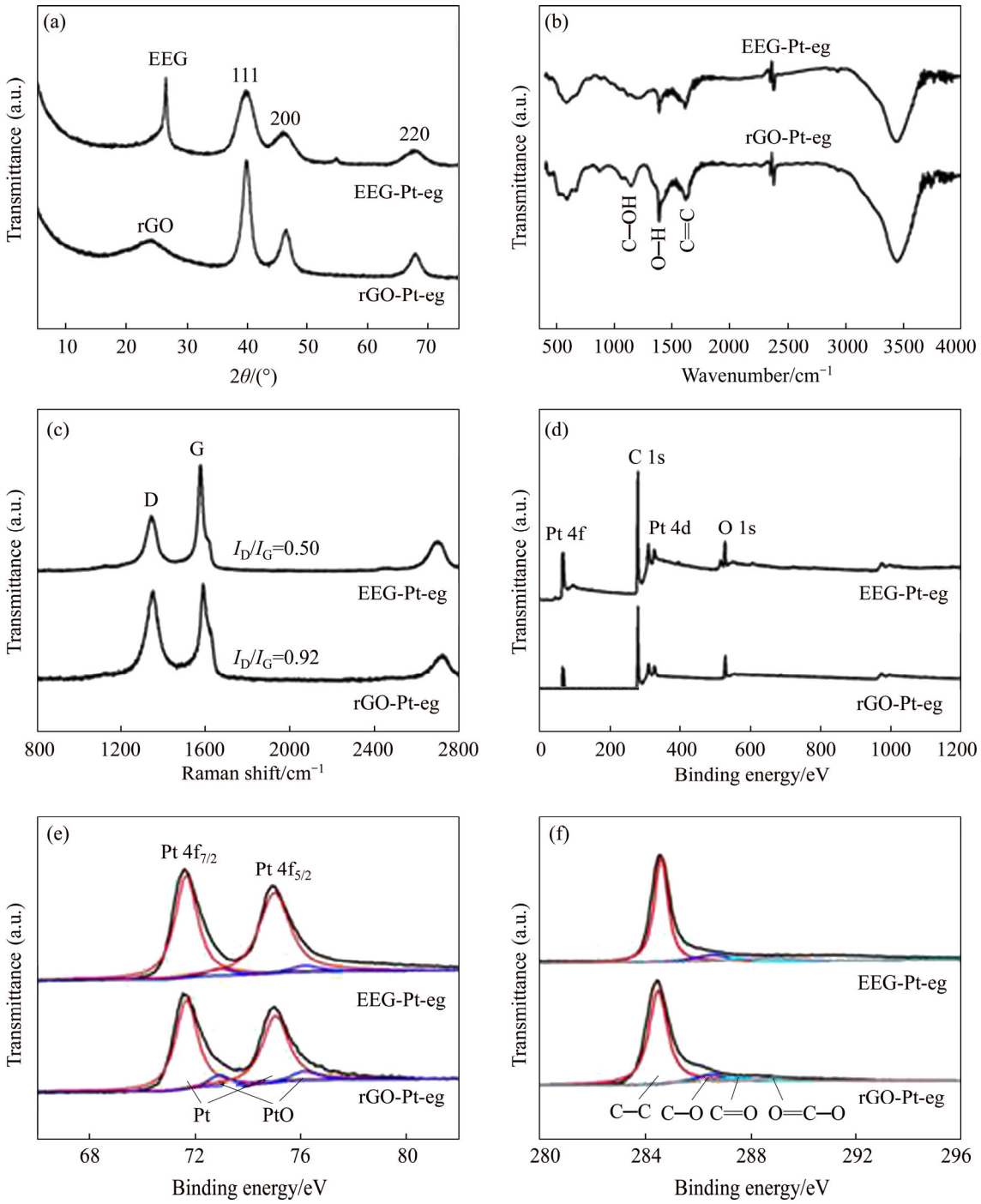

Figure 3 XRD patterns (The peaks in XRD patterns are indexed onto the cubic phase of Pt with a=0.3878 nm) (a), FT-IR (b), Raman (c), XPS survey (d), high-resolution Pt 4f XPS (e), high-resolution C 1s XPS spectra (f) of EEG-Pt-eg and rGO-Pt-eg

a 0.5 mol/L H_2SO_4 solution by cyclic voltammetry (CV). The ECSAs are calculated by the integration of the hydrogen adsorption region in CV curves (Figure 4(a)) [28, 29]. EEG-Pt-eg has much higher ECSA (216.5 cm^2/mg) than rGO-Pt-eg (159.8 cm^2/mg), which can be attributed to the smaller size of Pt particles on EEG, and the higher electrical conductivity of EEG as the catalyst support. CV curves of these samples (Figure 4(b)) were recorded in a solution of 0.5 mol/L H_2SO_4 and 1 mol/L CH_3OH. The CV peak emerging in the forward scan reflects the oxidation of methanol, and accordingly, the forward peak current (I_f) can evaluate the electrocatalytic activity of Pt catalysts for methanol oxidation. Another peak emerging in the reverse scan reflects the elimination of the

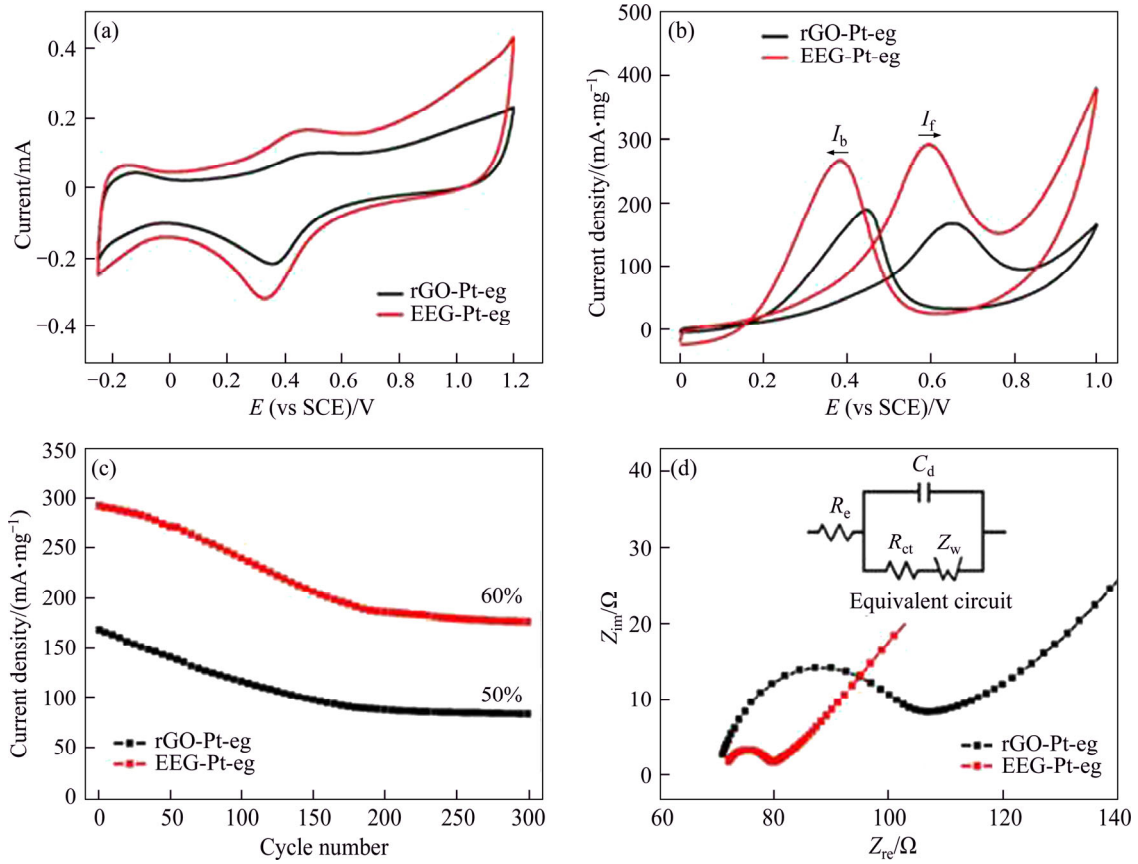

Figure 4 CV curves of EEG-Pt-eg and rGO-Pt-eg in N_2-saturated 0.5 mol/L H_2SO_4 (a), 0.5 mol/L H_2SO_4 and 1 mol/L CH_3OH at a scan rate of 50 mV/s (b), forward peak current densities of EEG-Pt-eg and rGO-Pt-eg as a function of cycle number for methanol oxidation (c), electrochemical impedance spectra of EEG-Pt-eg and rGO-Pt-eg in 0.5 mol/L H_2SO_4 and 1 mol/L CH_3OH (d) (The inset of (d) is equivalent circuit used to fit impedance spectra)

residual carbonaceous species (e.g., CO) that are left in the forward scan. Thus the ratio of the forward peak current to the backward peak current (I_f/I_b) can be used to estimate the tolerance of Pt catalysts against CO poisoning [30, 31]. The I_f value of EEG-Pt-eg is ~292.4 mA/mg_{Pt}, much higher than that of rGO-Pt-eg (~168.1 mA/mg_{Pt}), indicating that EEG-Pt-eg has better electrocatalytic activity than rGO-Pt-eg. Nevertheless, the I_f/I_b value of EEG-Pt-eg is only 1.09, slightly higher than rGO-Pt-eg (0.89). Although EEG as the catalyst support can drastically enhance the electrocatalytic activity of Pt nanoparticles, mass-generated carbonaceous intermediates could poison Pt catalysts to lose their activities after long-term cycling. The cyclic stability of EEG-Pt-eg and rGO-Pt-eg (Figure 4(c)) was tested in the same solution. The MOR performance of EEG-Pt-eg or rGO-Pt-eg decreases with the increase number of cycles, but it tends to be stable after 200 cycles. After 300 cycles, the I_f value of EEG-Pt-eg is maintained at ~176.2 mA/mg_{Pt}, still higher than that of rGO-Pt-eg (~83.2 mA/mg_{Pt}). However, the catalytic activity retention of EEG-Pt-eg (60%) still needs to be improved though it is higher than that of rGO-Pt-eg (50%).

To further validate the advantages of EEG as the catalyst support, EIS analysis of EEG-Pt-eg and rGO-Pt-eg is performed. As shown in Figure 4(d), Nyquist plots are comprised of a semicircle in the high frequency range and a sloping straight line in the low frequency range, which are associated with the charge transfer resistance (R_{ct}) and the Warburg impedance (Z_w), respectively [32, 33]. The R_{ct} values of EEG-Pt-eg and rGO-Pt-eg are 7.7 and 30.6 Ω, respectively, calculated by fitting curves with the equivalent circuit model (the inset of Figure 4(d)). The fast electron transfer from Pt catalysts to EEG guarantees the outstanding electrocatalytic performance of EEG-Pt-eg. All data concerned with the electrocatalytic properties are displayed in Table S1.

3.3 Structural and morphological characterization of EEG-SnO_2@Pt and EEG-SnO_2/Pt

Although EEG can raise the electrocatalytic activity of Pt nanoparticles, the severe CO poisoning of Pt catalysts still decreases the cyclic stability of EEG-Pt-eg. In our previous work [12], SnO_2 as a catalyst promoter can effectively raise the CO oxidation ability of Pt due to the adsorbed hydroxyl radical on the surface of SnO_2. The increased number of OH_{ads} facilitates the dissociative adsorption of methanol on the surface of Pt catalysts [20, 34]. Therefore, the electrocatalytic performance of EEG-Pt-eg could be further improved by cooperation with SnO_2. XRD pattern of EEG-SnO_2@Pt (Figure 5(a)) shows characteristic peaks which belong to the Pt and SnO_2 crystals respectively, indicating the successfully introduction of SnO_2 into EEG-Pt-eg. XPS survey spectrum of EEG-SnO_2@Pt (Figure 5(b)) further confirms the presence of SnO_2 because of the peaks of Sn 3p, Sn 3d and Sn 4d existing in the spectrum. The N 1s peak is hardly observed in the spectrum, suggesting that glycine is almost removed by washing. This brings SnO_2 nanoparticles in close contact with Pt nanoparticles. The high-resolution XPS spectra of EEG-SnO_2@Pt (Figure S4) show two main peaks at 71.6 and 74.9 eV that are ascribed to the Pt $4f_{7/2}$ and $4f_{5/2}$ of Pt^0, and two main peaks at 487.6 and 496.0 eV that are ascribed to the SnO_2.

By comparing SEM image of EEG-SnO_2@Pt (Figure 5(c)) with that of EEG-Pt-eg, it is found that many agglomerates are formed on EEG, implying that Pt catalysts are located around SnO_2 nanocrystals. The neighboring nanoparticles in the HRTEM image (Figure 5(d)) exhibit lattice spacings of ~0.226 and ~0.335 nm, agreeing well with the *d*-spacings of the (111) plane of Pt and the (110) plane of SnO_2, respectively. Forming Pt nanoparticles (solid white circle) around SnO_2

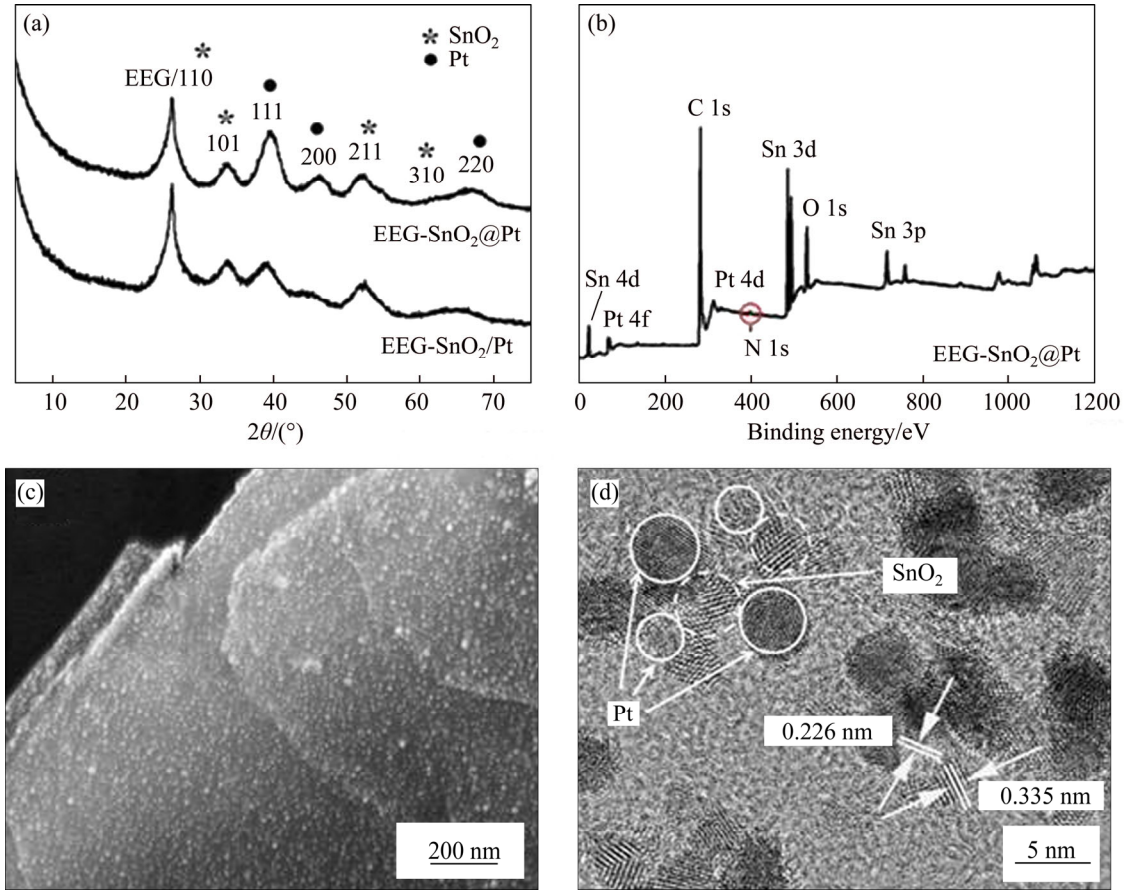

Figure 5 (a) XRD patterns of EEG-SnO_2@Pt and EEG-SnO_2/Pt (The peaks in XRD patterns are indexed onto cubic phase of Pt with *a*=0.3878 nm, marked by "•", and the tetragonal phase of SnO_2 with *a*=0.4751 nm and *c*=0.3197 nm, marked by "*", respectively); (b) XPS survey spectrum of EEG-SnO_2@Pt; (c) SEM and (d) HRTEM images of EEG-SnO_2@Pt (The *d*-spacings of the marked fringes in (d) are ca. 0.226 and 0.335 nm, corresponding to the (111) plane of cubic Pt and the (111) plane of tetragonal SnO_2, respectively)

nanoparticles (dotted white circle) is beneficial to oxidization of carbonaceous intermediates with hydroxyl radicals and improving the poison tolerance of Pt catalysts. To study the necessity of the connection between Pt and SnO_2 nanoparticles, EEG-SnO_2/Pt was also synthesized without using glycine as a linker. It seems that Pt and SnO_2 crystals are more distributed on EEG in the SEM image (Figure S5(a)). HRTEM image (Figure S5(b)) reveals that Pt nanoparticles are randomly formed on SnO_2-docorated EEG without the help of glycine, leading to the separation of partial Pt and SnO_2 nanoparticles on EEG.

3.4 Electrochemical performance of EEG-SnO_2@Pt and EEG-SnO_2/Pt

The electrocatalytic properties of EEG-SnO_2@Pt and EEG-SnO_2/Pt were tested to explore the role of SnO_2 in the electrocatalysis. To avoid the interference of Pt and SnO_2 loadings, the loadings of Pt and SnO_2 in EEG-SnO_2@Pt are ~16.8 wt% and ~27.0 wt% respectively, very closed to those in EEG-SnO_2/Pt (~18.1 wt% and ~26.6 wt% respectively). CV curves (Figures 6(a) and (b)) show that the ECSA and I_f of EEG-SnO_2@Pt are 375.9 cm^2/mg and 431.3 mA/mg_{Pt}, much higher than those of EEG-Pt-eg (216.5 cm^2/mg and 292.4 mA/mg_{Pt}). EEG-SnO_2/Pt exhibits decreased ECSA and I_f (281.3 cm^2/mg and 397.8 mA/mg_{Pt}) because parts of Pt nanoparticles are not contacted with SnO_2 nanoparticles, but they are still higher than those of EEG-Pt-eg. EEG-SnO_2@Pt also displays higher I_f/I_b (2.07) than EEG-Pt-eg (1.09), indicating the enhanced poison tolerate of Pt catalysts promoted by SnO_2. Note that the I_f/I_b value of EEG-SnO_2/Pt (1.41) is not as good as EEG-SnO_2@Pt, illustrating that the close-contacted structure is required for improving the anti-poisoning ability of Pt catalysts. The electrocatalytic durability of EEG-SnO_2@Pt for methanol oxidation is also substantially improved (Figure 6(c)) and an I_f value of 360.3 mA/mg_{Pt} is

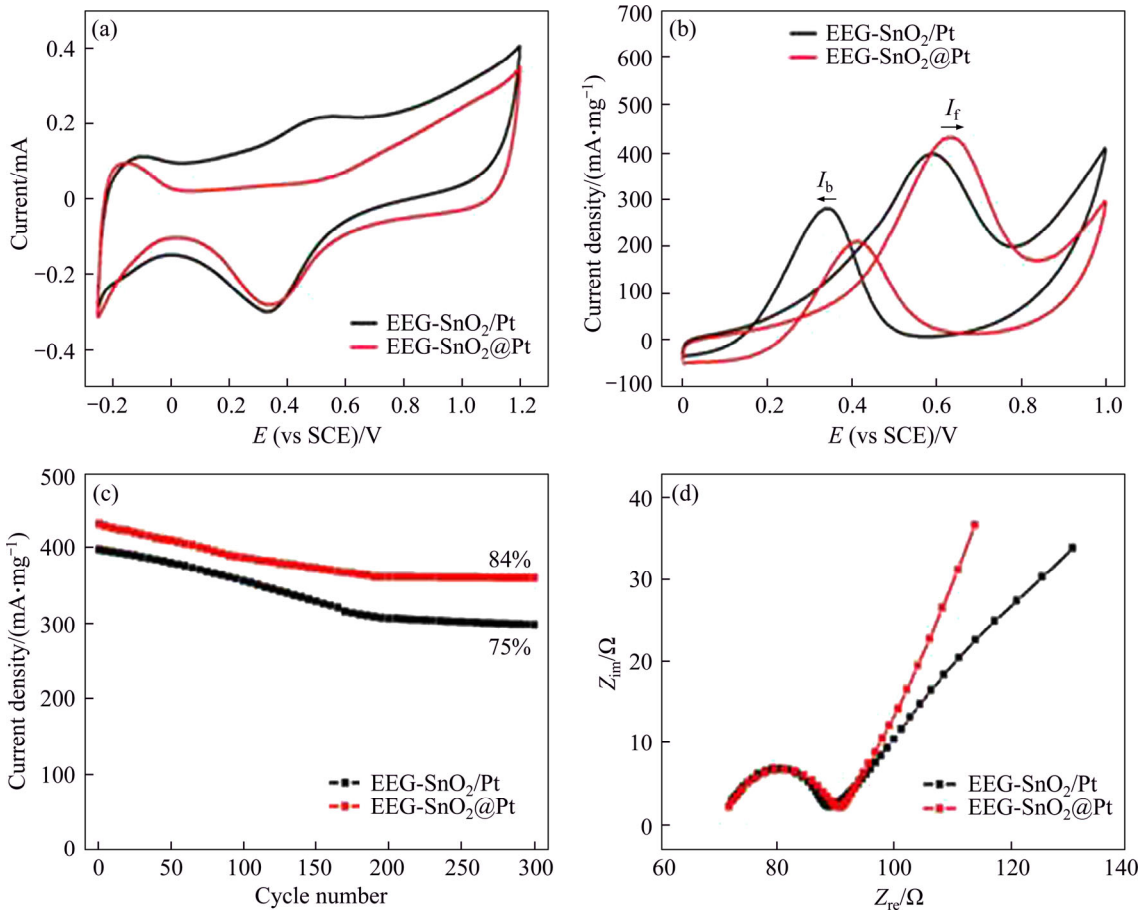

Figure 6 CV curves of EEG-SnO_2@Pt and EEG-SnO_2/Pt in N_2-saturated 0.5 mol/L H_2SO_4 (a) and 0.5 mol/L H_2SO_4 and 1 mol/L CH_3OH at a scan rate of 50 mV/s (b), forward peak current densities of EEG-SnO_2@Pt and EEG-SnO_2/Pt as a function of the cycle number for methanol oxidation (c), electrochemical impedance spectra of EEG-SnO_2@Pt and EEG-SnO_2/Pt in 0.5 mol/L H_2SO_4 and 1 mol/L CH_3OH (d)

achieved after 300 cycles with a retention of 84%. EEG-SnO_2/Pt shows an I_f value of 298.8 mA/mg_{Pt} after 300 cycles with a retention of 75%. The MOR performance comparison of EEG-Pt-eg and EEG-SnO_2@Pt with reported graphene-based Pt composites is summarized in Table S2.

The EIS measurements (Figure 6(d)) indicate that EEG-SnO_2@Pt and EEG-SnO_2/Pt have similar charge transfer resistances (15.7 and 15.1 Ω), which are both higher than that of EEG-Pt-eg (7.7 Ω). The increased R_{ct} values are ascribed to the introduction of SnO_2 into EEG-Pt-eg. Although the presence of SnO_2 reduces the electrical conductivity of EEG-SnO_2@Pt, the electrocatalytic properties of EEG-SnO_2@Pt are still substantially increased, proving that the anti-poisoning ability is a significant factor affecting the electrocatalytic activity of Pt catalysts. In addition, the close-contacted structure of EEG-SnO_2@Pt is also important to give full play to the function of SnO_2.

4 Conclusions

We described the successful preparation of ultra-small Pt nanoparticles on the EEG substrate by using ethylene glycol as both the solvent and the reducing agent. Compared to Pt nanocrystals on rGO, Pt nanocrystals on EEG show smaller particle size, better dispersion and antioxidant ability. Accordingly, EEG-Pt-eg exhibits better MOR performance than rGO-Pt-eg. In addition, EEG displays great electrical and mechanical properties owing to its intact graphene structure, which also contributes to the superior electrocatalytic performance of EEG-Pt-eg. To inhibit the CO poisoning of Pt catalysts, SnO_2 as a catalyst promoter is introduced into EEG-Pt-eg. It is found that the contact of Pt catalysts with SnO_2 is very important for the improvement of electrocatalytic performance. Considering the outstanding properties of EEG as a catalyst support, EEG-Pt-eg and EEG-SnO_2@Pt are promising to replace the commercial Pt/C as advanced anode catalysts for DMFCs.

Supporting information

1 Preparation of EEG

Natural graphite flakes were used as anode for electrochemical exfoliation of graphite. A Pt wire was used as a cathode. The electrolyte for the exfoliation was prepared by dissolving ammonium sulfate in aqueous solution (0.1 mol/L). The distance between the graphite and the Pt electrode was ~2 cm and was kept constant throughout the electrochemical process. Electrochemical exfoliation was carried out by applying positive voltage (10 V) to the graphite electrode. After the graphite exfoliation was completed, the product was collected through a polytetrafluoroethylene (PTFE) membrane filter with 0.2 μm pore size and washed several times with deionized water by vacuum filtration. The resultant EEG was then dispersed in DMF by sonication for 2 h. The dispersion was maintained for at least 48 h to precipitate un-exfoliated graphite flakes and particles, and the top solution was used for materials synthesis.

2 Synthesis of GO

GO was synthesized from natural graphite powders by a modified Hummer's method. In a typical synthesis, 5 g of graphite powder and 5 g of $NaNO_3$ were added into 230 mL of 98% H_2SO_4 under stirring in an ice bath. 30 g of $KMnO_4$ was slowly added to the mixture under stirring for 15 min below 5 °C. The mixture was then heated at 35 °C for 30 min. Subsequently, 460 mL of distilled water was slowly added into the above mixture, followed by stirring the mixture at 98 °C for more than 15 min. The mixture was further diluted with 1400 mL of distilled water and the reaction was terminated by adding 25 mL of 30% H_2O_2. Meanwhile, the color of the solution turned from dark brown to bright yellow. The resulting mixture was filtered and washed with distilled water several times to remove residual acids and salts. As-prepared GO was dispersed in water by ultrasonication for 30 min, followed by a low-speed centrifugation to get rid of any aggregated GO nanosheets.

3 Sample characterization

Specimens were characterized using X-ray diffraction (XRD) on a Phillips X'pert Pro MPD diffractometer with Cu K_α radiation and X'Pert HighScore Plus was used as the analysis software. Fourier transform infrared (FT-IR) spectra were recorded on a Nicolet-380 Fourier-transform infrared spectrometer. X-ray photoelectron (XPS) spectra were recorded on a Shimadzu Axis Ultra

spectrometer with Mg K_α radiation and XPS Peak Fit was used as the fitting software. Raman scattering spectra were recorded on a Jobin-Yvon Laser Confocal Micro-Raman Spectrometer with a 633 nm laser source. The contents in specimens were analyzed by ICP atomic emission spectroscopy (Jarrel-ASH, ICAP-9000) after specimens were dissolved in an aqua regia solution. Further characterization was performed by using field emission scanning electron microscopy (FESEM) on a Hitachi S-8010 electron microscope at an accelerating voltage of 10 kV, transmission electron microscopy (TEM) and high-resolution TEM (HRTEM) on a JEOL JEM-2011 electron microscope operating at 200 kV. SEM, TEM and HRTEM images were recorded at 60k, 94k and 630k magnifications, respectively. Energy-dispersive X-ray microanalysis (EDX) attached in an electron microscope was used to qualitatively determine the present elements and their distributions. The electrical conductivities of specimens were measured by a four-point probe set up from a Keithley 2400 source meter.

4 Electrocatalytic measurements

The electrochemical properties of Pt-containing specimens were measured by cyclic voltammetry in a standard three-electrode cell using CHI 700E electrochemical workstation. The three-electrode cell consisted of a saturated calomel electrode (SCE) serving as the reference electrode, a Pt wire serving as the counter electrode, and a catalyst-coated glassy carbon electrode (GCE) serving as the working electrode. The SCE needs to be calibrated before used. Briefly, the new SCE and the SCE which needs to be calibrated were placed in the saturated potassium chloride solution and connected to the voltmeter. Ensuring that the value of voltmeter is within ±2 mV and kept for a long time. The electrochemically active surface areas of specimens were measured by cyclic voltammetry in a 0.5 mol/L H_2SO_4 solution at a scan rate of 50 mV/s. The electrocatalytic activities and durability of specimens were studied by performing cyclic voltammetry in a solution containing 0.5 mol/L H_2SO_4 and 1.0 mol/L CH_3OH at a scan rate of 50 mV/s. Electrochemical impedance spectra (EIS) measurements were performed by using a Gamry Interface 1000 electrochemical workstation and applying a sine wave over the frequency range from 10^6 to 0.01 Hz in a solution containing 0.5 mol/L H_2SO_4 and 1.0 mol/L CH_3OH. All electrochemical tests were performed in N_2-saturated electrolyte which was obtained by bubbling N_2 gas through the electrolyte for at least 30 min before testing.

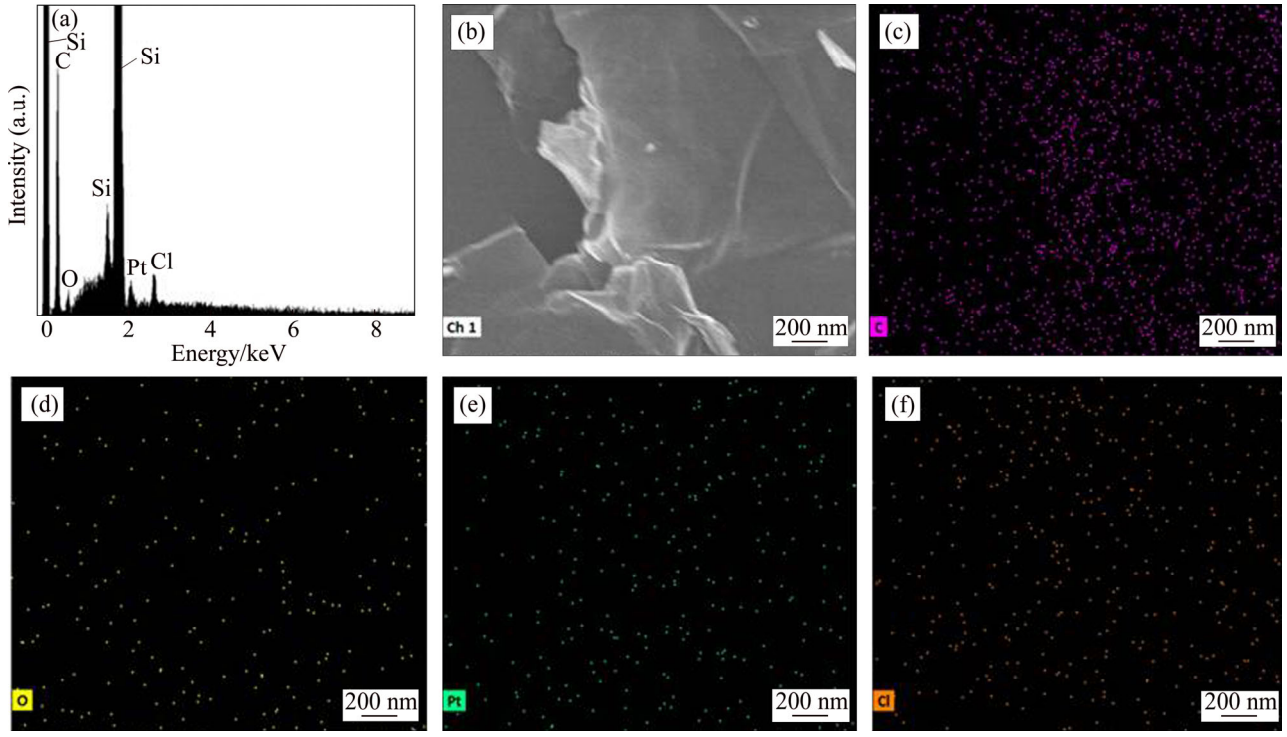

Figure S1 EDX spectrum (a) and SEM-EDX mapping images (b−f) of EEG-H_2PtCl_6

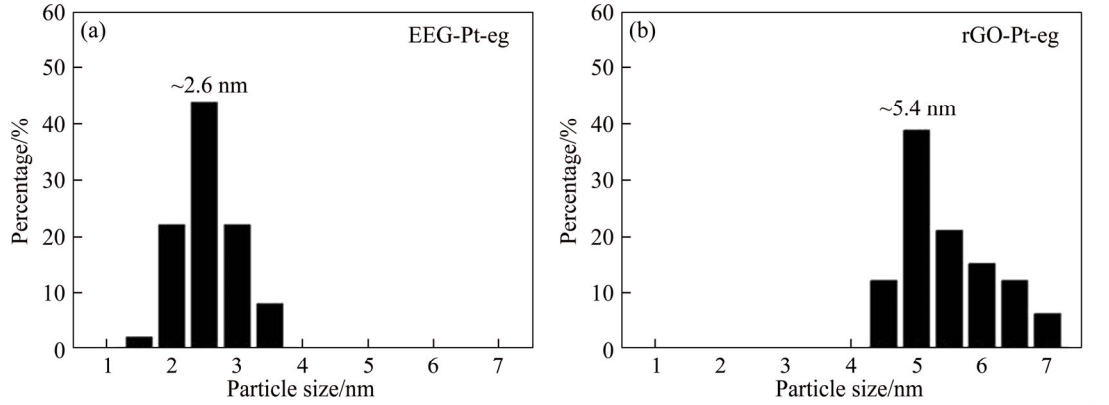

Figure S2 Particle size distribution histograms of Pt catalysts on EEG (a) and rGO (b)

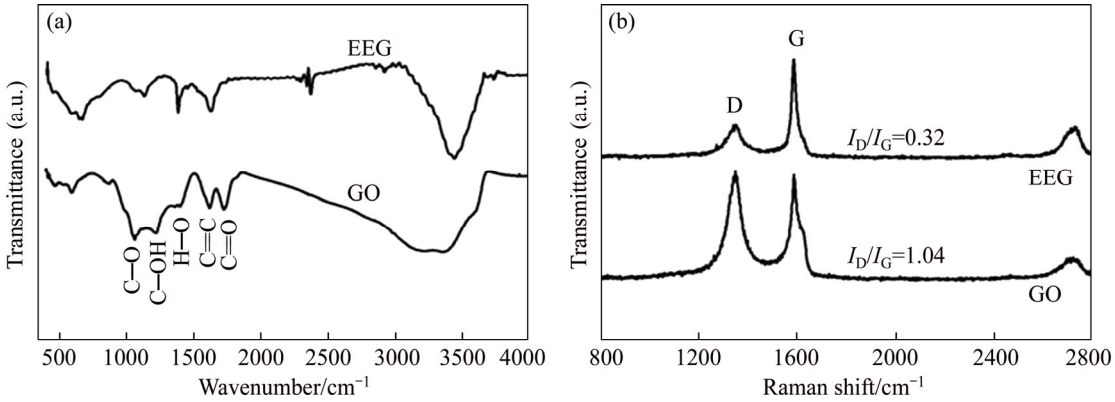

Figure S3 FT-IR (a) and Raman spectra (b) of GO and EEG

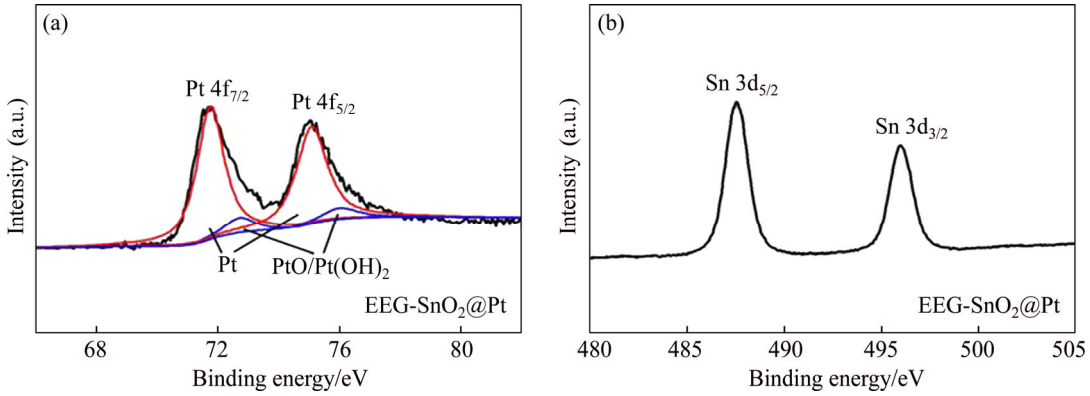

Figure S4 High-resolution Pt 4f (a) and high-resolution Sn 3d XPS spectra (b) of EEG-SnO_2@Pt

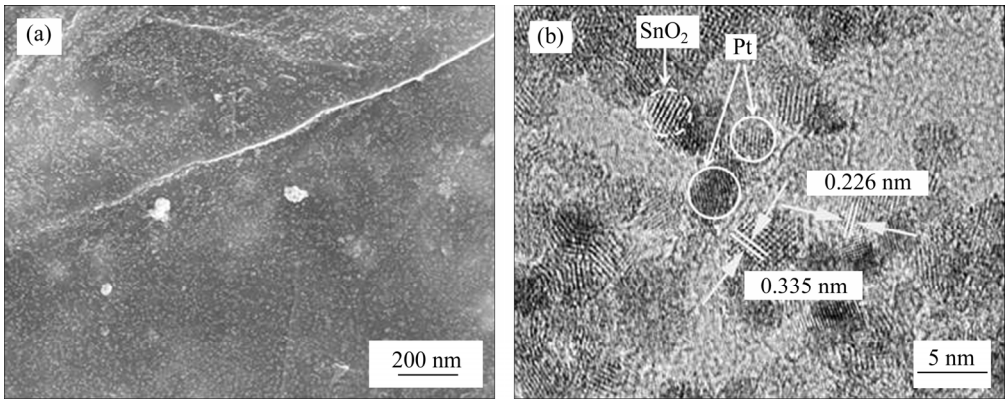

Figure S5 SEM (a) and HRTEM images (b) of EEG-SnO_2/Pt

Table S1 Mean particle sizes and contents of Pt in EEG-Pt-eg, rGO-Pt-eg, EEG-SnO_2@Pt and EEG-SnO_2/Pt and their ECSAs, forward peak current densities (I_f), I_f/I_b ratios and R_{ct} values

Sample	Particle size of Pt/nm	Pt content in mass fraction/%	SnO_2 content in mass fraction/%	ECSA/ ($cm^2 \cdot mg^{-1}$)	I_f/($mA \cdot mg_{Pt}^{-1}$)	I_f/I_b	R_{ct}/Ω
EEG-Pt-eg	2.6	17.6	N/A	216.5	292.4	1.09	7.7
rGO-Pt-eg	5.4	18.3	N/A	159.8	168.1	0.89	30.6
EEG-SnO_2@Pt	2.8	16.8	27.0	375.9	431.3	2.07	15.7
EEG-SnO_2/Pt	3.5	18.1	26.6	281.3	397.8	1.41	15.1

Table S2 Summary of MOR performance of reported graphene-supported Pt hybrids

Sample	w(Pt)/%	I_f/($mA \cdot mg_{Pt}^{-1}$)	I_f/I_b	Reference
Pt/rGO	N/A	350.5	1.1	Chem. Commun. 2015, 51: 2418. [35]
Pt/3D graphene	N/A	93.3	1.3	J. Power Sources 2015, 273: 624 [36]
Pt/graphene	31	202.2	1.4	J. Phys. Chem. C 2014, 118: 1182 [37]
Pt/rGO	N/A	333.3	~1	ACS Appl. Mater. Interfaces 2015, 7: 22935 [38]
Pt@graphene	20	195	<1	Chem. Commun. 2010, 46: 5951 [39]
Pt/Pys-graphene	20	279.5	1.4	Electrochim. Acta 2013, 111: 275 [40]
Pt/graphene	40	~265	<1	Carbon 2011, 49: 904 [41]
EEG-Pt-eg	17.6	292.4	1.1	This work
EEG-SnO_2@Pt	16.8	431.3	2.1	This work

Contributors

YUAN Xu: Investigation, methodology, writing-original draft. ZHANG Jin: Investigation, validation. YUE Wen-bo: Supervision, conceptualization, writing-reviewing & editing, funding acquisition.

Conflict of interest

The authors declare that they have no known competing financial interests or personal relationships that could have appeared to influence the work reported in this paper.

References

[1] LIU Min-min, ZHANG Rui-zhong, CHEN Wei. Graphene-supported nanoelectrocatalysts for fuel cells: Synthesis, properties, and applications [J]. Chem Rev, 2014, 114: 5117−5160. DOI: 10.1021/cr400523y.

[2] LONG Gui-fa, LI Xiao-hua, WAN Kai, LIANG Zhen-xing, PIAO Jin-hua, TSIAKARAS P. Pt/$C_{N\text{-doped}}$ electrocatalysts: Superior electrocatalytic activity for methanol oxidation reaction and mechanistic insight into interfacial enhancement [J]. Appl Catal B: Environ, 2017, 203: 541−548. DOI: 10.1016/j.apcatb.2016.10.055.

[3] KIM D H, SHIN D Y, LEE Y G, AN G H, HAN J H, AHN H J, CHOI B J. Effects of SnO_2 layer coated on carbon nanofiber for the methanol oxidation reaction [J]. Ceram Int, 2018, 44: 19554−19559. DOI: 10.1016/j.ceramint.2018.07.199.

[4] WANG Li-ping, TIAN Jing, LI Jing-sha, ZENG Xian-guang, PENG Zhi-guang, HUANG Xiao-bing, TANG You-gen, WANG Hai-yan. Red-blood-cell-like nitrogen-doped porous carbon as an efficient metal-free catalyst for oxygen reduction reaction [J]. J Cent South Univ, 2019, 26: 1459−1468. DOI: https://doi.org/10.1007/s11771-019-4102-y.

[5] CHEN Tsan-yao, HUANG Po-chun, LIAO Yen-fa, LIU Yu-ting, TEH Tsung-kuang, LIN Tsang-lang. Shell thickness effects on reconfiguration of NiO_{core}–Pt_{shell} anodic catalysts in a high current density direct methanol fuel cell [J]. RSC Adv, 2016, 6: 72607−72615. DOI: 10.1039/c6ra17013g.

[6] XIA Zhang-xun, XU Xin-long, ZHANG Xiao-ming, LI Huan-qiao, WANG Su-li, SUN Gong-quan. Anodic engineering towards high-performance direct methanol fuel cells with non-precious-metal cathode catalysts [J]. J Mater Chem A, 2020, 8: 1113−1119. DOI: 10.1039/c9ta11440h.

[7] NAN Li-rui, YUE Wen-bo, JIANG Yang. Fabrication of graphene-porous carbon–Pt nanocomposites with high electrocatalytic activity and durability for methanol oxidation [J]. J Mater Chem A, 2015, 3: 22170−22175. DOI: 10.1039/c5ta06854a.

[8] ZHANG Yang-ping, GAO Fei, SONG Ping-ping, WANG Jin, SHIRAISHI Y, DU Yu-kou. Glycine-assisted fabrication of N-Doped graphene-supported uniform multipetal PtAg nanoflowers for enhanced ethanol and ethylene glycol oxidation [J]. ACS Sustainable Chem Eng, 2019, 7: 3176−3184. DOI: 10.1021/acssuschemeng.8b05020.

[9] QIN Yong, CHAO Lei, YUAN Jie, LIU Yang, CHU

Fu-qiang, KONG Yong, TAO Yong-xie, LIU Mei-lin. Ultrafine Pt nanoparticle-decorated robust 3D N-doped porous graphene as an enhanced electrocatalyst for methanol oxidation [J]. Chem Commun, 2016, 52: 382−385. DOI: 10.1039/c5cc07482g.

[10] HE Yuan, LIU Yun-guo. Direct fabrication of highly porous graphene/TiO_2 composite nanofibers by electrospinning for photocatalytic application [J]. J Cent South Univ, 2018, 25: 2182−2189. DOI: https://doi.org/10.1007/s11771-018-3906-5.

[11] ZHU Cheng-zhou, WANG Ping, WANG Li, HAN Lei, DONG Shao-jun. Facile synthesis of two-dimensional graphene/SnO_2/Pt ternary hybrid nanomaterials and their catalytic properties [J]. Nanoscale, 2011, 3: 4376−4382. DOI: 10.1039/c1nr10634a.

[12] GAO Li-na, YUE Wen-bo, TAO Shan-shan, FAN Lou-zhen. Novel strategy for preparation of Graphene-Pd, Pt composite, and its enhanced electrocatalytic activity for alcohol oxidation [J]. Langmuir, 2013, 29: 957−964. DOI: 10.1021/la303663x.

[13] QU Yun-teng, GAO Yun-zhi, WANG Long, RAO Jian-cun, YIN Ge-ping. Mild synthesis of Pt/SnO_2/graphene nanocomposites with remarkably enhanced ethanol electro-oxidation activity and durability [J]. Chem Eur J, 2016, 22: 193−198. DOI: 10.1002/chem.201503867.

[14] WEI Wei, WANG Gang, YANG Sheng, FENG Xin-liang, MULLEN K. Efficient coupling of nanoparticles to electrochemically exfoliated graphene [J]. J Am Chem Soc, 2015, 137: 5576−5581. DOI: 10.1021/jacs.5b02284.

[15] CHEN Chia-hsuan, YANG Shiou-wen, CHUANG Min-chiang, WOON Wei-yen, SU Ching-yuan. Towards the continuous production of high crystallinity graphene via electrochemical exfoliation with molecular in situ encapsulation [J]. Nanoscale, 2015, 7: 15362−15373. DOI: 10.1039/c5nr03669k.

[16] YANG Sheng, BRULLER S, WU Zhong-shuai, LIU Zhao-yang, PARVEZ K, DONG Ren-hao, RICHARD F, SAMORI P, FENG Xin-liang, MULLEN K. Organic radical-assisted electrochemical exfoliation for the scalable production of high-quality graphene [J]. J Am Chem Soc, 2015, 137: 13927−13932. DOI: 10.1021/jacs. 5b09000.

[17] YANG Sheng, LOHE M R, MULLEN K, FENG Xin-liang. New-generation graphene from electrochemical approaches: Production and applications [J]. Adv Mater, 2016, 28: 6213−6221. DOI: 10.1002/adma.201505326.

[18] XU Ze-xuan, YUE Wen-bo, LIN Rong, CHIANG Chang-yang, ZHOU Wu-zong. Direct growth of SnO_2 nanocrystallites on electrochemically exfoliated graphene for lithium storage [J]. J Energy Storage, 2019, 21: 647−656. DOI: 10.1016/j.est.2019.01.001.

[19] XU Ze-xuan, ZHANG Ping, CHEN Jia-lu, YUE Wen-bo, ZHOU Wu-zong. Growth and growth mechanism of oxide nanocrystals on electrochemically exfoliated graphene for lithium storage [J]. Energy Storage Mater, 2019, 18: 174−181. DOI: 10.1016/j.ensm.2018.08.023.

[20] NAN Li-rui, FAN Ze-tan, YUE Wen-bo, DONG Qiao, ZHU Li-sha, YANG Liu, FAN Lou-zhen. Graphene-based porous carbon-Pd/SnO_2 nanocomposites with enhanced electrocatalytic activity and durability for methanol oxidation [J]. J Mater Chem A, 2016, 4: 8898−8904. DOI: 10.1039/c6ta01416j.

[21] ZHANG Jun, LIU Xiang-hong, GUO Xian-zhi, WU Shi-hua, WANG Shu-rong. A general approach to fabricate diverse noble-metal (Au, Pt, Ag, Pt/Au)/Fe_2O_3 hybrid nanomaterials [J]. Chem Eur J, 2010, 16: 8108−9700. DOI: 10.1002/chem.201000096.

[22] YANG Sheng, RICCIARDULLI A G, LIU Shao-hua, DONG Ren-hao, LOHE M R, BECKER A, SQUILLACI M A, SAMORI P, MULLEN K, FENG Xin-liang. Ultrafast delamination of graphite into high-quality graphene using alternating currents [J]. Angew Chem Int Ed, 2017, 56: 6669−6675. DOI: 10.1002/anie.201702076.

[23] TURGUT H, TIAN Z R, YU Feng-jiao, ZHOU Wu-zong. Multivalent cation cross-linking suppresses highly energetic graphene oxide's flammability [J]. J Phys Chem C, 2017, 121: 5829−5835. DOI: 10.1021/acs.jpcc.6b13043.

[24] ZHAO Peng, YUE Wen-bo, YUAN Xu, BAO Hua-ying. Exceptional lithium anodic performance of Pd-doped graphene-based SnO_2 nanocomposite [J]. Electrochim Acta, 2017, 225: 322−329. DOI: 10.1016/j.electacta.2016.12.124.

[25] LI Zhong-shui, XU Shu-hong, XIE Yi-xie, WANG Yan-lin, LIN Shen. Promotional effects of trace Bi on its highly catalytic activity for methanol oxidation of hollow Pt/graphene catalyst [J]. Electrochim Acta, 2018, 264: 53−60. DOI: 10.1016/j.electacta.2018.01.096.

[26] CHEN Ke, ZHANG Fei, SUN Jing-yu, LI Zhen-zhu, ZHANG Li, BACHMATIUK A, ZOU Zhi-yu, CHEN Zhao-long, ZHANG Li-ya, RUMMELI M H, LIU Zhong-fan. Growth of defect-engineered graphene on manganese oxides for Li-ion storage [J]. Energy Storage Mater, 2018, 12: 110−118. DOI: 10.1016/j.ensm.2017.12.001.

[27] PARVEZ K, WU Zhong-shuai, LI Rong-jin, LIU Xian-jie, GRAF R, FENG Xin-liang, MULLEN K. Exfoliation of graphite into graphene in aqueous solutions of inorganic salts [J]. J Am Chem Soc, 2014, 136: 6083−6091. DOI: 10.1021/ja5017156.

[28] CHU Yuan-yuan, ZHANG Ning, YANG Jing-jing, WANG Hai-tao, DAI Zhao, WANG Liang, GAO Jun, TAN Xiao-yao. Designed synthesis of thin CeO_2 nanowires-supported Pt electrocatalysts with pore-interconnected structure and its high catalytic activity for methanol oxidation [J]. J Mater Sci, 2018, 53: 2087−2101. DOI: 10.1007/s10853-017-1636-y.

[29] FENG Yuan-yuan, BI Li-xiao, LIU Zeng-hua, KONG De-sheng, YU Zhang-yu. Significantly enhanced electrocatalytic activity for methanol electro-oxidation on Ag oxide-promoted PtAg/C catalysts in alkaline electrolyte [J]. J Catal, 2012, 290:18−25. DOI: 10.1016/j.jcat.2012.02.013.

[30] YANG Pei-pei, YUAN Xiao-lei, HU Hui-cheng, LIU Yi-lin, ZHENG Hao-wen, YANG Di, CHEN Lei, CAO Mu-han, XU Yong, MIN Yu-lin, LI Yan-guang, ZHANG Qiao. Solvothermal synthesis of alloyed ptni colloidal nanocrystal clusters (CNCs) with enhanced catalytic activity for methanol oxidation [J]. Adv Funct Mater, 2018, 28: 1704774. DOI: 10.1002/adfm.201704774.

[31] QIAN Wen, HAO Rui, ZHOU Jian, EASTMAN M, MANHAT B A, SUN Qiang, GOFORTH A M, JIAO Jun. Exfoliated graphene-supported Pt and Pt-based alloys as electrocatalysts for direct methanol fuel cells [J]. Carbon, 2013, 52: 595−604. DOI: 10.1016/j.carbon.2012.10.031.

[32] NAN Li-rui, YUE Wen-bo. Exceptional electrocatalytic activity and selectivity of platinum@Nitrogen-doped mesoporous carbon nanospheres for alcohol oxidation [J]. ACS Appl Mater Interfaces, 2018, 10: 26213−26221. DOI: 10.1021/acsami.8b06347.

[33] DU De-jian, DU Yi-en, YUE Wen-bo, YANG Xiao-jing. Lithium storage performance of {010}-faceted and [111]-faceted anatase TiO_2 nanocrystals [J]. J Cent South Univ, 2019, 26: 1530−1539. DOI: https://doi.org/10.1007/s11771-019-4109-4.

[34] WU Shou-liang, LIU Jun, LIANG De-wei, SUN Hong-mei, YE Yi-xing, TIAN Zhen-fei, LIANG Chang-hao. Photo-excited in situ loading of Pt clusters onto rGO immobilized SnO_2 with excellent catalytic performance toward methanol oxidation [J]. Nano Energy, 2016, 26: 699−707. DOI: 10.1016/j.nanoen.2016.06.038.

[35] FENG Hong-bin, LIU Yong, LI Jing-hong. Highly reduced graphene oxide supported Pt nanocomposites as highly efficient catalysts for methanol oxidation [J]. Chem Commun, 2015, 51: 2418−2420. DOI: 10.1039/c4cc09146a.

[36] WANG Ming-jun, SONG Xue-fen, YANG Qi, HUA Hao, DAI Shu-ge, HU Chen-guo, WEI Da-peng. Pt nanoparticles supported on graphene three-dimensional network structure for effective methanol and ethanol oxidation [J]. J Power Sources, 2015, 273: 624−630. DOI: 10.1016/j.jpowsour.2014.09.117.

[37] ZHAO Jian, YU Hui, LIU Zhen-sheng, JI Min, ZHANG Li-qing, SUN Guang-wei. Supercritical deposition route of preparing Pt/Graphene composites and their catalytic performance toward methanol electrooxidation [J]. J Phys Chem C, 2014, 118: 1182−1190. DOI: 10.1021/jp402620p.

[38] WU Shou-liang, LIU Jun, TIAN Zhen-fei, CAI Yun-yu, YE Yi-xing, YUAN Qing-lin, LIANG Chang-hao. Highly dispersed ultrafine pt nanoparticles on reduced graphene oxide nanosheets: in situ sacrificial template synthesis and superior electrocatalytic performance for methanol oxidation [J]. ACS Appl Mater Interfaces, 2015, 7: 22935−22940. DOI: 10.1021/acsami.5b06153.

[39] ZHOU Yi-ge, CHEN Jing-jing, WANG Feng-bin, SHENG Zhen-huan, XIA Xing-hua. A facile approach to the synthesis of highly electroactive Ptnanoparticles on graphene as an anode catalyst for direct methanolfuelcells [J]. Chem Commun, 2010, 46: 5951−5953. DOI: 10.1039/c0cc00394h.

[40] LIANG Qing-sheng, ZHANG Li, CAI Mao-lin, LI Yong, JIANG Kun, ZHANG Xin, SHEN Pei-kang. Preparation and charaterization of Pt/functionalized graphene and its electrocatalysis for methanol oxidation [J]. Electrochim Acta, 2013, 111:275−283. DOI: 10.1016/j.electacta.2013.07.198.

[41] CHOI Sung-mook, SEO Min-ho, KIM Hyung-ju, KIM Won-bae. Synthesis of surface-functionalized graphene nanosheets with high Pt-loadings and their applications to methanol electrooxidation [J]. Carbon, 2011, 49: 904−909. DOI: 10.1016/j.carbon.2010.10.055.

(Edited by YANG Hua)

中文导读

电化学剥离石墨烯作为高性能催化剂载体促进甲醇在铂催化剂上的电催化氧化

摘要：电化学剥离石墨烯是一种高质量的石墨烯，其表面几乎没有含氧官能团和缺陷，因此比其他碳材料(例如广泛使用的还原氧化石墨烯)更适合作为催化剂载体。然而，由于石墨烯的惰性表面，其功能材料很难在电化学剥离的石墨烯上生长。在这项工作中，超小的 Pt 纳米晶(~2.6 nm)成功地生长在电化学剥离的石墨烯表面，对甲醇氧化的电催化活性优于还原氧化石墨烯负载的 Pt 催化剂。电化学剥离石墨烯负载的铂催化剂具有优异的电催化性能，这主要归功于电化学剥离石墨烯与铂之间的快速电子转移，同时，电化学剥离石墨烯负载的铂催化剂具有颗粒尺寸小、分散性高、氧化态 Pt 含量低等优点。此外，利用甘氨酸作为连接剂，在电化学剥离石墨烯上可以控制铂催化剂周围生成 SnO_2 纳米晶，进一步增强铂催化剂的抗中毒能力。电化学剥离石墨烯具有良好的导电性和机械强度，有望作为新型催化剂载体得到广泛应用。

关键词：电化学剥离石墨烯；铂；二氧化锡；甘氨酸；甲醇氧化